AIAA JOURNAL
Vol. 34, No. 1, January 1996

Flap–Lag–Torsion Stability in Hover and Forward Flight with Three-Dimensional Wake

A. R. Manjunath*
Hindustan Aeronautics Limited, Bangalore 560017, India
S. J. Chunduru†
Florida Atlantic University, Boca Raton, Florida 33431
J. Nagabhushanam‡
Indian Institute of Science, Bangalore 560012, India
and
G. H. Gaonkar§
Florida Atlantic University, Boca Raton, Florida 33431

The contributions of full-wake dynamics in trim analysis are demonstrated for finding the control inputs and periodic responses simultaneously, as well as in Floquet eigenanalysis for finding the damping levels. The equations of flap bending, lag bending, and torsion are coupled with a three-dimensional, finite state wake, and low-frequency (<1/rev) to high-frequency (>1/rev) multiblade modes are considered. Full blade-wake dynamics is used in trim analysis and Floquet eigenanalysis. A uniform cantilever blade in trimmed flight is investigated over a range of thrust levels, advance ratios, number of blades, and blade torsional frequencies. The investigation includes the convergence characteristics of control inputs, periodic responses, and damping levels with respect to the number of spatial azimuthal harmonics and radial shape functions in the wake representation. It also includes correlation with the measured lag damping of a three-bladed untrimmed rotor. The parametric study shows the dominant influence of wake dynamics on control inputs, periodic responses, and damping levels, and wake theory generally improves the correlation.

Nomenclature

a = lift-curve slope, 1/rad
C_{d0} = profile drag coefficient
C_l = lift coefficient
C_T = thrust coefficient
C_T/σ = blade loading or thrust level
$\bar{f}$ = equivalent flat plate area of parasite drag
i = blade number
j = polynomial number
$[L_c]$, $[L_s]$ = influence coefficient matrices
L_i = circulatory lift per unit span of the ith blade, N/m
M = highest m
m = harmonic number
$[M]$ = mass matrix
n = polynomial number
Q = number of blades
R = rotor radius, m
r = harmonic number
$\bar{r}_i$ = radial distance measured from rotor center for the ith blade
S = number of radial shape functions per harmonic
t = time
V = inflow parameter
$[V]$ = diagonal matrix with elements $V_t, V, V, \ldots, V$
V_t = total inflow
α = airfoil section angle of attack
α_s = shaft-tilt angle, rad and deg
α_j^r, β_j^r = wake states
β_1, β_2 = first and second mode flap response
γ = Lock number
ζ_1, ζ_2 = first and second mode lag response
$\theta_0, \theta_c, \theta_s$ = collective, lateral cyclic, and longitudinal cyclic pitch angles, respectively, rad and deg
λ_t = total inflow
$\lambda(\bar{r}_i, \psi_i, t)$ = downwash on the ith blade
λ_m = thrust-induced inflow
μ = advance ratio
ρ = air density, kg/m^3
σ = rotor solidity
τ_n^{mc}, τ_n^{ms} = cosine and sine components of the inflow forcing function
$\phi_j^r(\bar{r}_i)$ = radial shape function
ϕ_1, ϕ_2 = first and second mode torsional response
ψ_i = azimuthal location of the ith blade, rad
ω_β = nondimensional rotating first flap frequency
ω_ζ = nondimensional rotating first lag frequency
ω_ϕ = nondimensional rotating first torsion frequency
Ω = rotor speed, rad/s
$(\cdot)$ = $()/\mathrm{d}t$

Received Nov. 1, 1994; revision received July 5, 1995; accepted for publication Aug. 10, 1995.

*Chief Manager (Design), Helicopter Design Bureau.
†Graduate Research Assistant, Department of Mechanical Engineering.
‡Professor, Department of Aerospace Engineering.
§Professor, Department of Mechanical Engineering. Associate Fellow AIAA.

Introduction

LAG or inplane modes are at best weakly damped, and their instabilities are potential problems of rotorcraft; indeed, the importance of lag damping has long been recognized.[1] Given the delicate balance of drag, induced drag, and Coriolis forces in the inplane direction, and the sensitivity of induced drag to unsteady downwash or wake, lag damping prediction requires an adequate dynamic wake representation. In the early 1980s Pitt and Peters[2] developed a low-frequency approximation of a dynamic wake from first principles in a state-variable form that lends itself well to perturbation about a trim or equilibrium position and thereby to the subsequent Floquet eigenanalysis, and the term dynamic inflow has become associated with it. The dynamic inflow model is simple to use; it has only three states. It has been used extensively in low-frequency flight dynamics studies including lag-damping prediction; for details see the review by

Gaonkar and Peters.[3] Some 10 years later Peters et al.[4] developed a comprehensive dynamic wake model as a closed-form solution to the complete three-dimensional potential-flow equations. Like dynamic inflow, dynamic wake is a finite state model and permits Floquet eigenanalysis. Unlike dynamic inflow, however, it is not restricted to low-frequency wake representation. In fact, it accounts for full-wake dynamics, both shed and trailing components, implicitly includes dynamic inflow, and captures Loewy's lift-deficiency theory.[4] More importantly, it correlates well with test data.[5] It has been discussed extensively in the literature as well (e.g., Refs. 4–7). Our objective is to predict lag damping in hover and forward flight with experimental correlation; to this end we use this three-dimensional finite state wake model and the Floquet theory, which is widely used and provides a rigorous basis for trimming and finding damping levels of rotorcraft.[8–10] Our objective is not to weigh the relative merits of different wake theories or to compare Floquet eigenanalysis with other methods of extracting damping levels, such as moving block analysis, which has been applied fruitfully in extracting damping levels from measured and predicted time histories. To put this paper in perspective, we briefly touch upon the difficulties associated with a wide range of wake models in Floquet eigenanalysis and the state of the art of computing lag-mode damping with full three-dimensional wake dynamics.

Lag-damping prediction requires adequate dynamic wake representation at all advance ratios, and dynamic inflow and lift-deficiency type representations, though widely used, are not adequate.[7] Predictions are also sensitive to blade modeling and to trim results of control inputs and periodic responses; see Johnson.[11] Moreover, this sensitivity and nonlinear interaction of the aerodynamic and structural states require balanced sophistication in modeling these states, as well as in extracting the trim results of control inputs and periodic responses and damping levels.[6] That is, all aerodynamic states often have to be included not only in trim analysis but also in Floquet eigenanalysis. This means vortex-filament type models, such as prescribed-wake and free-wake models (we bypass subdistinctions based on lifting-line and lifting-surface theories), are virtually precluded. Such models, notwithstanding their capacity to provide detailed wake histories and their proven usage in vibration and performance predictions, contain hidden states[12]; thus, they are not structured for finite state representation that is perturbed about a trim position.

Although routinely used in loads and vibration analysis, aeroelastic stability with three-dimensional wake is treated only in a few studies. Friedmann[13] proposes a finite state dynamic wake model in the time domain to approximate lift-deficiency type approaches, including Loewy's. Though a tractable approximation to an involved three-dimensional problem, this is only a two-dimensional approximation. Torok and Chopra[14] use a free-wake model to compute the trim results, but the wake is frozen in stability analysis. Thus, although wake dynamics is included in nonlinear trim analysis, it is not included during perturbation analysis of extracting damping levels. Kwon et al.[15] use a vortex-lattice wake model; they use the database presented by Sharpe[16] under hovering conditions and show that wake dynamics improves correlation. This correlation work in hover with Sharpe's database is further pursued by de Andrade and Peters[17] on the basis of the three-dimensional, finite state wake model of Ref. 4. The results corroborate the findings of Ref. 15 with a saving in computer time by a factor of 30. Manjunath et al.[7] use a rigid flap–lag model representation and the same three-dimensional, finite state wake model of Ref. 4; the results are restricted to untrim and moment-trim (vertical shaft, as in a wind-tunnel model) conditions and do not account for the important effects of flap bending, lag bending, and torsion. We also mention two related studies due to Yoo et al.[18] and due to Yoo[19]; both studies predict lag damping in hover from a vortex-lattice method using a moving block procedure, flap–lag–torsion model in Ref. 18 and a rigid flap–lag model in Ref. 19. Reference 19 also includes correlations with test data[20] and predictions from the dynamic inflow model; it is seen that the dynamic inflow model gives overall better correlation. Recently, Cho and Lee[21] studied the sensitivity of flap–lag–torsion stability to modeling assumptions in various unsteady two-dimensional theories including Loewy's lift-deficiency function. As seen, it is a two-dimensional approximation of a three-dimensional phenomenon, restricted to hover, and such lift-deficiency type approaches include only shed vorticity.

Overall, it is seen that only the barest beginnings have been made, particularly in forward flight. With this background, this paper advances the state of the art of predicting lag damping with three-dimensional dynamic wake in the following respects.

1) It investigates the convergence characteristics of trim results and damping levels with respect to the number of spatial azimuthal harmonics and radial shape functions in the wake representation; both low-frequency (<1/rev) and high-frequency (>1/rev) multiblade modes are included. The investigation is based on full Floquet analysis in that all structural and aerodynamic states are included from modeling to trim analysis to eigenanalysis.

2) A comprehensive parametric study is provided to isolate the effects of dynamic wake on trim results and damping levels of all blade modes, such as the low-frequency first lag mode to the high-frequency second torsion mode. It covers four rotor configurations with three to six blades and includes a range of thrust levels, advance ratios, and torsional frequencies. We emphasize that the number of blades is an important parameter because it affects shed vorticity and thereby the alignment of the vortex layers below the rotor.[7]

3) It includes correlation with the measured lag damping under hovering and forward flight conditions. Specifically, an appreciable section of the database of Ref. 20 is selected, for which dynamic stall is not a major issue. The correlation demonstrates both the strengths and the weaknesses of predicting lag damping.

Modeling and Analysis

To facilitate discussion of results, we begin with a brief account of modeling the blade and the flowfield, particularly the root-flexure-blade assembly of the experimental rotor and the downwash. The results are based on three aerodynamic theories, which also are spelled out explicitly. This is followed by a mention of the derivation of the state equations, trim analysis, and Floquet eigenanalysis.

Structural Modeling

Four isolated rotors with three to six blades are considered. The convergence and parametric studies of wake effects on trim results and damping levels are based on a cantilever blade model. The correlation with test data refers to a three-bladed untrimmed rotor.[20] The airfoil or the blade portion of the experimental rotor has essentially uniform mass and stiffness distributions, but the root flexure has highly nonuniform mass and stiffness distributions, and its modeling affects damping prediction.[22] Accordingly, the correlation in Ref. 23 is based on three structural models that differ in approximating the root-flexure portion of the experimental rotor. The predictions from all three structural approximations are identical at low advance ratios; however, they show some sensitivity to structural modeling at high advance ratios where the thrust level is relatively high. But, these differences are minor when dynamic stall is not a major issue.[23] In the present study, we show the correlation based on only one structural model, in which actual mass and stiffness distributions of the root-flexure-blade assembly are used to calculate the mode shapes. The database refers to full flap–lag structural coupling (pitch change takes place inboard of the root flexure) as well as to zero flap–lag structural coupling (pitch change takes place outboard of the root flexure). The root-flexure model used in the present correlation study accounts for such flap–lag structural coupling details. For additional details, see Ref. 23.

Aerodynamics

The airfoil aerodynamics uses linear quasisteady theory and includes reverse-flow and large angle-of-attack effects on lift.[24] Quasisteady stall, dynamic stall, and compressibility effects are neglected. The finite state downwash model represents a closed-form solution to the complete, three-dimensional potential-flow equations and accounts for the finite number of blades.[4] We consider an ith blade with azimuthal location ψ_i. At a blade station with radial coordinate $\bar{r}_i$, the inflow $\lambda(\bar{r}_i, \psi_i, t)$ is expanded in terms of

the azimuthal harmonics [$\cos(r\psi_i)$ and $\sin(r\psi_i)$] and radial shape functions $\phi_j^r(\bar{r}_i)$,

$$\lambda(\bar{r}_i, \psi_i, t) = \sum_{r=0}^{\infty} \sum_{j=r+1,r+3}^{\infty} \phi_j^r(\bar{r}_i) \times \left[\alpha_j^r(t)\cos(r\psi_i) + \beta_j^r(t)\sin(r\psi_i)\right] \quad (1)$$

The radial shape functions $\phi_j^r(\bar{r}_i)$ that account for the radial variation of the inflow are defined as

$$\phi_j^r(\bar{r}_i) = (1/\nu)\bar{P}_j^r(\nu) \quad (2)$$

where $\bar{P}_j^r$ is the normalized, associated Legendre's polynomial of the first kind. On the rotor disk, the ellipsoidal coordinate ν is related to the radial distance $\bar{r}_i$ as

$$\nu = \sqrt{1 - \bar{r}_i^2} \quad (3)$$

On expanding Eq. (2), the radial shape functions reduce to simple polynomial functions in $\bar{r}_i$ (for details, see Refs. 4 and 5).

As seen from Eq. (1), the inflow is expressed as a double summation in harmonic number r and polynomial number j. The harmonics can be truncated at any desired number (say, M). Concerning the number of radial shape functions associated with each harmonic, we fix the number of shape functions with each harmonic to a constant; that is, $S = \text{const}$. To illustrate, we set $S = 3$. For the zeroth harmonic we have three radial shape functions: ϕ_1^0, ϕ_3^0, and ϕ_5^0. Similarly, we have three radial shape functions for the first harmonic (ϕ_2^1, ϕ_4^1, and ϕ_6^1), three radial shape functions for the second harmonic (ϕ_3^2, ϕ_5^2, and ϕ_7^2), and so on. We note that with each radial shape function for zeroth harmonic we have one wake state and for each nonzero harmonic we have two wake states: one cosine state and one sine state. For example, with $S = 3, M = 6$, the wake representation, as detailed in Refs. 4–7, leads to 39 wake states: {(6 cosine states + 6 sine states + 1 zeroth harmonic state) per radial shape function} × {3 radial shape functions per harmonic}.

In Eq. (1), the cosine and sine components $\alpha_j^r(t)$ and $\beta_j^r(t)$ represent a finite set of states that act like degrees of freedom and are governed by the state equations

$$[M]\{\dot{\alpha}_j^r\} + [V][L_c]^{-1}\{\alpha_j^r\} = 0.5\{\tau_n^{mc}\} \quad (4)$$

$$[M]\{\dot{\beta}_j^r\} + [V][L_s]^{-1}\{\beta_j^r\} = 0.5\{\tau_n^{ms}\} \quad (5)$$

where $[V]$ is the diagonal matrix of flow parameters V_t and V; the first or the (1, 1) element is $V_t = \sqrt{(\mu^2 + \lambda_t^2)}$ and all other elements are $V = [\mu^2 + (\lambda_t + \lambda_m)\lambda_t]/\sqrt{(\mu^2 + \lambda_t^2)}$. The mass matrix $[M]$ is diagonal, and closed-form expressions are available for mass matrix $[M]$ and influence-coefficient matrices $[L_c]$ and $[L_s]$; see Refs. 4–6 for details. Similarly, on the right sides, τ_n^{mc} and τ_n^{ms} are cosine and sine components of the pressure expansion or inflow forcing functions that couple the wake dynamics with the blade structural dynamics. For a Q-bladed rotor, these are given by

$$\tau_n^{0c} = \frac{1}{2\pi}\sum_{i=1}^{Q}\int_0^1 \frac{L_i\phi_n^0(\bar{r}_i)}{\rho\Omega^2R^3}\,d\bar{r}_i \quad (6a)$$

$$\tau_n^{mc} = \frac{1}{\pi}\sum_{i=1}^{Q}\int_0^1 \frac{L_i\phi_n^m(\bar{r}_i)}{\rho\Omega^2R^3}\,d\bar{r}_i\cos(m\psi_i) \quad (6b)$$

$$\tau_n^{ms} = \frac{1}{\pi}\sum_{i=1}^{Q}\int_0^1 \frac{L_i\phi_n^m(\bar{r}_i)}{\rho\Omega^2R^3}\,d\bar{r}_i\sin(m\psi_i) \quad (6c)$$

We use the following three aerodynamic theories.

Linear theory: The lift, drag, and pitching moment are based on quasisteady linear aerodynamics; that is, lift coefficient $C_l = a\sin\alpha\cos\alpha$, and constant drag and pitching-moment coefficients. Inflow is assumed to be uniform and is calculated from a momentum theory.

Dynamic wake theory: The lift, drag, and pitching moment are the same as in the linear theory. The downwash dynamics, however, is described by Eq. (1) and is calculated from the finite state wake model given by Eqs. (4–6).

Dynamic inflow theory: The lift, drag, and pitching moment are the same as in the linear theory. The downwash dynamics is based on the widely used Pitt and Peters[2] model of dynamic inflow. It has three wake states with first harmonic inflow description and linear radial variation of inflow.

Equations of Motion

We use Hamilton's principle and second-order ordering scheme to derive the equations of flap bending, lag bending, and torsion, following the treatment given in Ref. 25. These are nonlinear integropartial differential equations with periodic coefficients. The orthogonal nonrotating mode shapes are used to eliminate the spatial

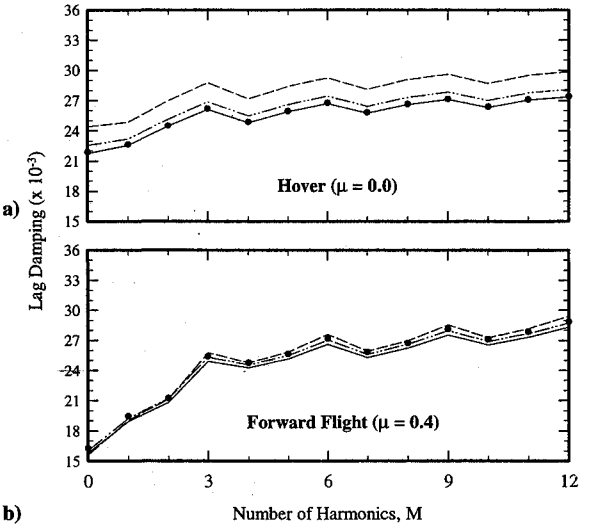

Fig. 1 Oscillatory convergence of lag damping of the regressive mode with respect to number of harmonics of wake states and blade modes for $\mu = 0.0$ and 0.4, $C_T/\sigma = 0.2$, and $S = 3$: L-F-T; ----, 1-1-1; —·—·—, 2-3-1; ———, 2-2-2; ●, 3-3-3.

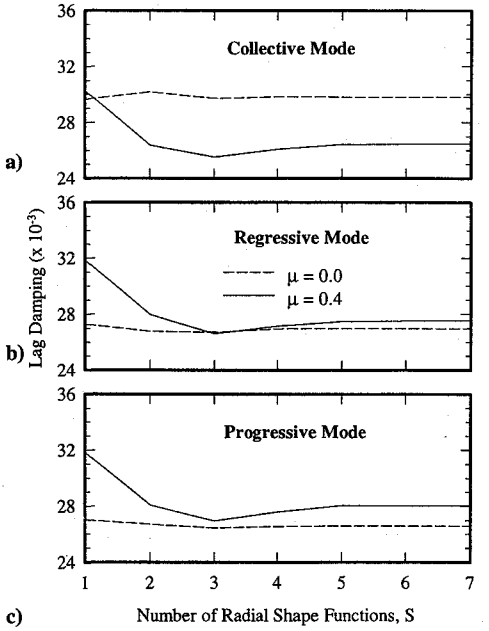

Fig. 2 Effect of number of radial shape functions with each harmonic on lag damping of the multiblade modes for $C_T/\sigma = 0.2$ and $M = 6$.

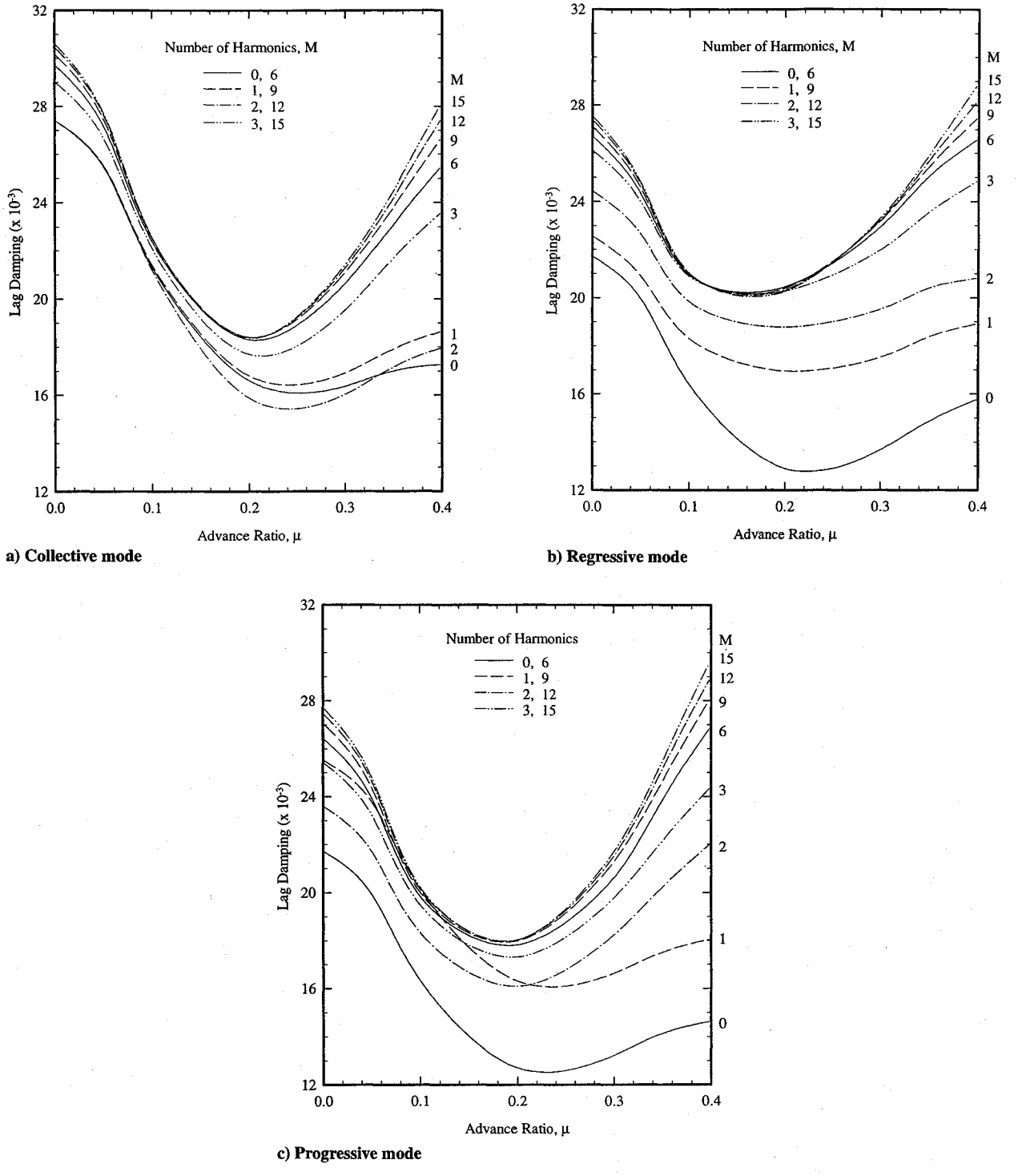

a) Collective mode

b) Regressive mode

c) Progressive mode

Fig. 3 Lag damping of the multiblade modes vs advance ratio with increasing number of harmonics of wake states for $C_T/\sigma = 0.2$ and $S = 3$.

dependency and to obtain the ordinary differential equations in nondimensional time. For the cantilever blade model, modal representation is a routine exercise. For the experimental blade, the nonrotating modes are obtained numerically. In passing we mention that for the cantilever blade model, rotating modes also were used. Damping predictions from both type of modes were found to be virtually identical.

An appealing aspect of finite state wake representation is the simplicity of coupling the blade equations with the full-wake dynamics as in earlier lag-damping predictions with dynamic inflow.[3] This coupling is recently elaborated by Manjunath et al.[7] for a rigid flap–lag problem and Peters and Su[26] for a flap-bending problem. Application to the present flap–lag–torsion problem essentially follows Refs. 7 and 26.

Analysis

The analysis is conveniently described in two parts. The first part refers to propulsive or flight trim and to Floquet eigenanalysis. The second part refers to the correlation with the measured lag damping of a three-bladed rotor, operated untrimmed. In flight trim, we compute the trim results of control inputs for the required flight conditions and the corresponding initial conditions for periodic response; the control inputs are collective pitch angle θ_0, lateral cyclic pitch angle θ_c, longitudinal cyclic pitch angle θ_s, and shaft-tilt angle α_s. The trim results are computed simultaneously by periodic shooting; the resulting nonlinear equations are solved by a damped Newton iteration scheme.[9] Unlike in Ref. 9, however, in which an optimal Newton damping parameter is calculated over each iteration, we use a fixed value of 0.7 throughout. No divergence

problem was encountered. In the experimental study,[20] the blades were set for prescribed collective pitch angle θ_0 and shaft-tilt angle α_s prior to each run; thus, the control inputs are known and periodic shooting refers to finding the periodic response. The damping levels are routinely computed from eigenanalysis of the Floquet transition matrix (FTM) that is generated as a byproduct of trim analysis.

Results

The results are presented in three phases. Phase one in Figs. 1–9 addresses the wake- and blade-modeling details necessary for converged results of trim and damping levels, and phase two in Figs. 10–13 presents a parametric study of stability margins. Both phases cover a range of system parameters, such as advance ratio, thrust level, number of blades, and torsional frequency. Unless otherwise indicated, Figs. 1–13 are based on a 2-2-2 model (two nonrotating or rotating modes each in lag bending, flap bending, and torsion) with the following baseline values: $\mu = 0$ and 0.4, $Q = 3$, $C_T/\sigma = 0.1$ and 0.2, $\sigma = 0.05$, $a = 6.28$, $\gamma = 5$, $\omega_\beta = 1.15$, $\omega_\zeta = 0.7$, $\omega_\phi = 5.0$, $C_{d0} = 0.01$, $\bar{f} = 0.01$, $M = 9$, and $S = 3$. Moreover, for convenience, we refer to damping levels of the multiblade modes of a three-bladed rotor with respect to first lag-bending degree of freedom simply as lag damping of multiblade modes: regressive, collective, and progressive modes. Whenever we refer to multiblade modes of other degrees of freedom, such as second lag bending of a three-bladed rotor or multiblade modes of rotors with $Q = 4$, 5, and 6, these modes are explicitly identified. Although in some cases the choice of $C_T/\sigma = 0.2$, and to some extent $\mu = 0.4$, is not the most representative of a trimmed flight, it does represent a demanding case to test the adequacy of blade-wake modeling for converged results.

The correlation with the measured lag damping of the regressive mode of a three-bladed rotor is taken up in phase three in Figs. 14 and 15. Since the dynamic stall effects are not included, the correlation is limited to lightly and moderately loaded sections ($C_T/\sigma \leq 0.1$) of the database[20] for which dynamic stall is not a major issue. The correlation covers a section of the database with zero flap–lag structural coupling; the rotor speed $\Omega = 1000$ rpm and the corresponding nondimensional lead-lag frequency $\omega_\zeta = 0.61$.

Convergence Characteristics

As seen from Eq. (1), wake modeling involves a complete set of shape functions $\phi_j^r(\bar{r}_i)$ and spatial harmonics $\cos(r\psi_i)$ and $\sin(r\psi_i)$; shape functions account for radial variation and harmonics account for azimuthal variation. Thus, it is required that a sufficient number of shape functions and harmonics be included for convergence of trim results and damping levels. In combination with such a comprehensive wake representation, it is required equally that a balanced sophistication be maintained in blade modal representation of lag bending, flap bending, and torsion for convergence. A comprehensive study is carried out on convergence of trim results and damping levels with respect to blade modal expansion over a range of advance ratios and thrust levels with varying degrees of wake modeling. A section of these results is presented in Fig. 1a for hover and in Fig. 1b for forward fligt with $\mu = 0.4$; in both figures we consider a three-bladed rotor and a high-thrust condition with $C_T/\sigma = 0.2$. The lag damping of the regressive mode is shown for different combinations of blade modal representations. (For lag damping of the collective and progressive modes, see Ref. 23.) These results show that a 2-2-2 blade model is adequate for predicting lag damping of all three multiblade modes in hover and forward flight.

Convergence of damping levels with respect to the number of shape functions with each harmonic and of harmonics in the wake representation is explored in Figs. 2–6. We present all 18 multiblade modes: regressive, collective, and progressive modes of a three-bladed rotor with respect to each of the six degrees of freedom in the 2-2-2 blade model. The regressive, collective, and progressive first-lag modes are covered in Figs. 2–5, and the remaining multiblade modes in Fig. 6. In particular, Fig. 2 shows lag damping of the multiblade modes vs the number of radial shape functions for a preset value of six harmonics; that is, $M = 6$. As we mentioned earlier while presenting Eq. (1), the wake representation with three radial shape functions per harmonic (i.e., $S = 3$) and with six harmonics (i.e., $M = 6$) leads to 39 wake states and gives reasonably converged results from hover to high-speed cruising with $\mu = 0.4$; the higher is the advance ratio, the slower is the convergence. For example, the error with respect to $M = 6$ and $S = 7$ is less than 3% throughout. Basically similar results (not shown) are obtained for other preset values of M (e.g., $M = 9$). Therefore, henceforth, we take three radial shape functions per harmonic ($S = 3$) in the wake representation.

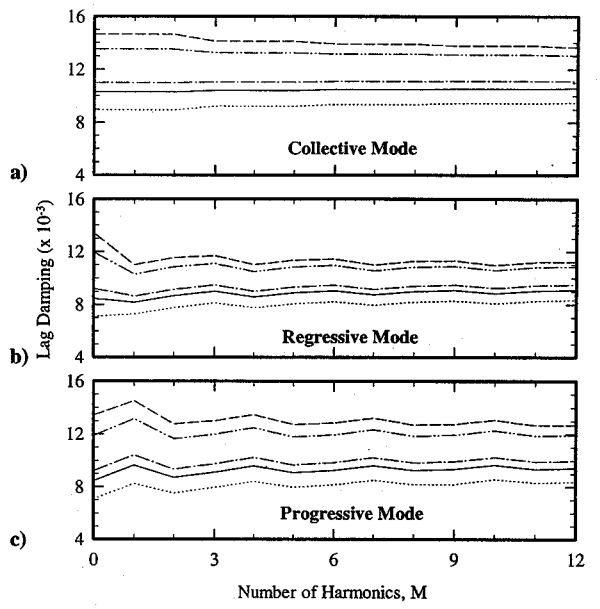

Fig. 4 Oscillatory convergence of lag damping of the multiblade modes with respect to number of harmonics of wake states for different torsional frequencies with $\mu = 0.0, C_T/\sigma = 0.1$, and $S = 3$: Torsional frequency (ω_ϕ) ----, 2.0; —·—·—, 2.5; —·—·—, 4.0; ———, 5.0; · · · ·, L-F.

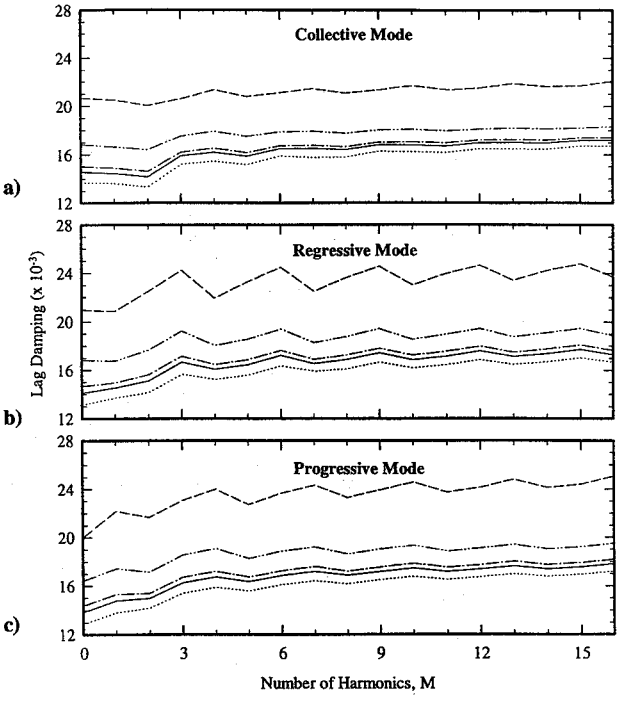

Fig. 5 Oscillatory convergence of lag damping of the multiblade modes with respect to number of harmonics of wake states for different torsional frequencies with $\mu = 0.4, C_T/\sigma = 0.1$, and $S = 3$; legend same as in Fig. 4.

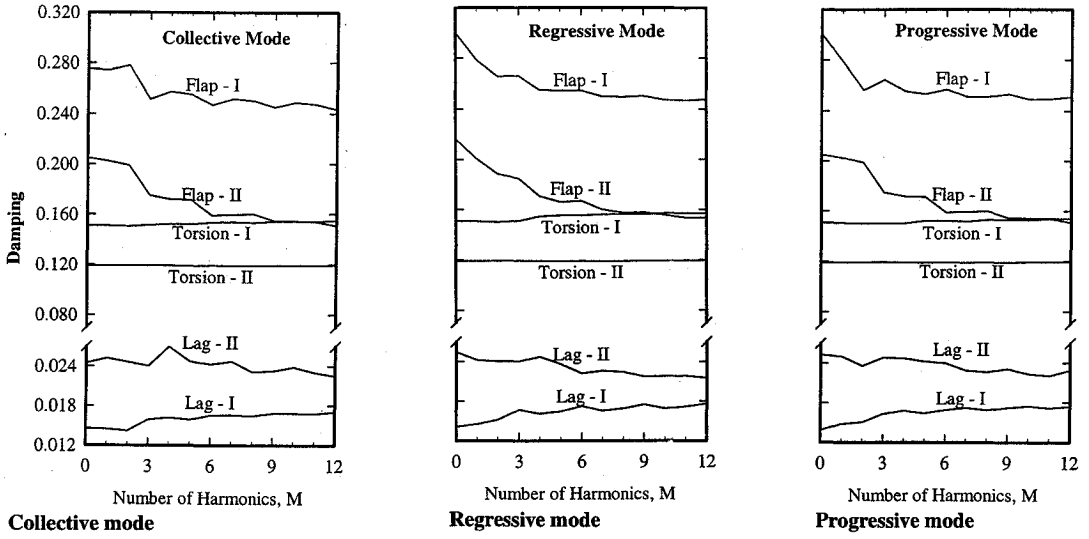

Fig. 6 Convergence of flap–lag–torsion damping of the multiblade modes with increasing number of harmonics of wake states for $\mu = 0.4$, $C_T/\sigma = 0.1$, and $S = 3$.

Figures 3a–3c show the convergence of lag damping of the multiblade modes over advance ratio for discrete values of M. Though busy figures, they show that damping of all three multiblade modes essentially converge for $M = 9$. For example, at $\mu = 0.3$, compared to the predictions with $M = 15$, the errors with respect to the collective mode in Fig. 3a, regressive mode in Fig. 3b, and progressive mode in Fig. 3c are less than 1%.

Given the sensitivity of lag-damping predictions to blade torsional flexibility, Fig. 4 in hovering and Fig. 5 at $\mu = 0.4$ show oscillatory convergence of lag damping of the multiblade modes vs M for different values of torsional frequency ω_ϕ. The L-F model therein represents the torsionally rigid case ($\omega_\phi \approx \infty$) with two modes each in lag bending and flap bending, a 2-2-0 modal representation. Figures 4 and 5 show that with increasing torsional flexibility (decreasing ω_ϕ), M or the number of harmonics in the wake representation for convergence increases for all three multiblade modes, both in hover and forward flight. For a specific value of ω_ϕ, more harmonics are required at $\mu = 0.4$ than in hovering for the same degree of convergence. This is generally true of all of the three multiblade modes. For example, at $\omega_\phi = 2.5$, lag damping of the regressive mode shows excellent convergence with $M = 8$ in hovering; for the same degree of convergence, $M = 12$ is required at $\mu = 0.4$.

Thus far, we investigated the convergence characteristics of damping of the first lag-bending mode. We now investigate similar convergence characteristics of the remaining multiblade modes of first and second flap bending and torsion, and second lag bending. This is done in Fig. 6, which also includes damping of all three multiblade modes of first lag bending to facilitate direct comparison. For completeness all 18 multiblade modes are shown. (The adequacy of the 2-2-2 modal representation for prediction of damping of the multiblade modes in second flap-bending, lag-bending, and torsion are discussed subsequently.) Overall, Fig. 6 demonstrates two points. First, reasonable convergence is obtained with $M = 9$, as was the case for lag damping of the multiblade modes. Second, compared with the results with $M = 0$ that roughly correspond to the no-dynamic-wake results, it is seen that dynamic wake is a significant contributor to the damping of all of the modes from the low-frequency first-lag regressive mode ($\omega \approx 0.3$ with $\omega_\zeta = 0.7$) to the high-frequency second-flap progressive mode ($\omega \approx 4.6$ with $\omega_\beta = 1.15$). An exception appears to be the torsion modes, in particular, the second torsion mode, which remains essentially unaffected by wake dynamics. This indicates that wake dynamics basically remains uncoupled with the second-torsion-mode dynamics.

As mentioned, the dynamic inflow model[2] is widely used in low-frequency flight dynamics studies, such as prediction of control inputs and lag damping. Therefore, a good question to ask is how dynamic inflow compares with a low-frequency approximation of

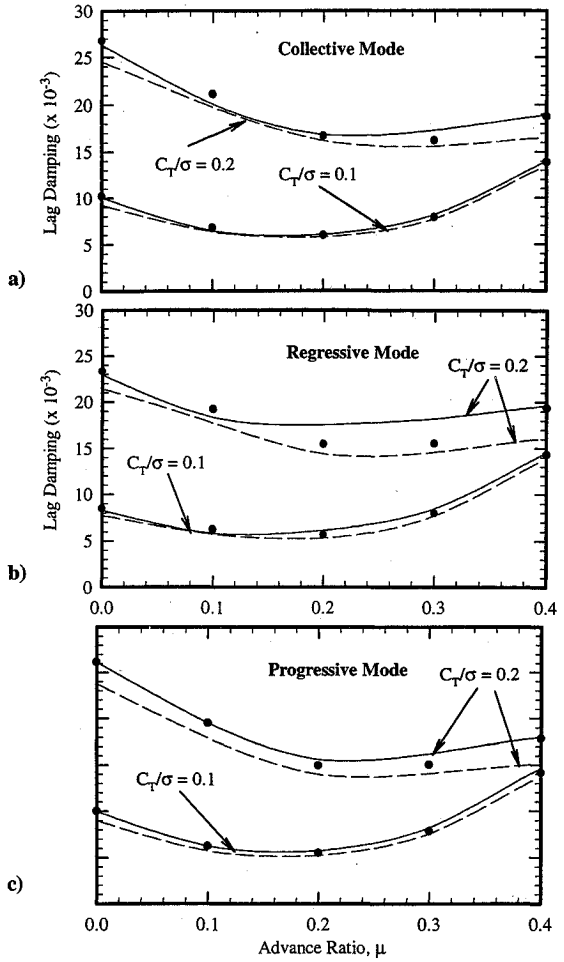

Fig. 7 Comparison of lag damping of the multiblade modes from dynamic wake ($M = 1, S = 1$) and dynamic inflow theories for $C_T/\sigma = 0.1$ and 0.2: ———, dynamic wake ($M = 1, S = 1$); — — ·, Pitt and Peters (trim by linear theory); ●, Pitt and Peters (trim by dynamic wake theory; $M = 1, S = 1$).

dynamic wake; that is, wake modeling with $M = 1$ and $S = 1$. Such a comparison is addressed in Fig. 7. As background, we mention that these two models are conceptually similar. In spite of differences in mass and influence-coefficient matrices, both are based on first-harmonic azimuthal variation and linear radial variation. Figure 7 shows lag damping of the multiblade modes for two cases of trim analysis, based on linear and dynamic wake theories, and

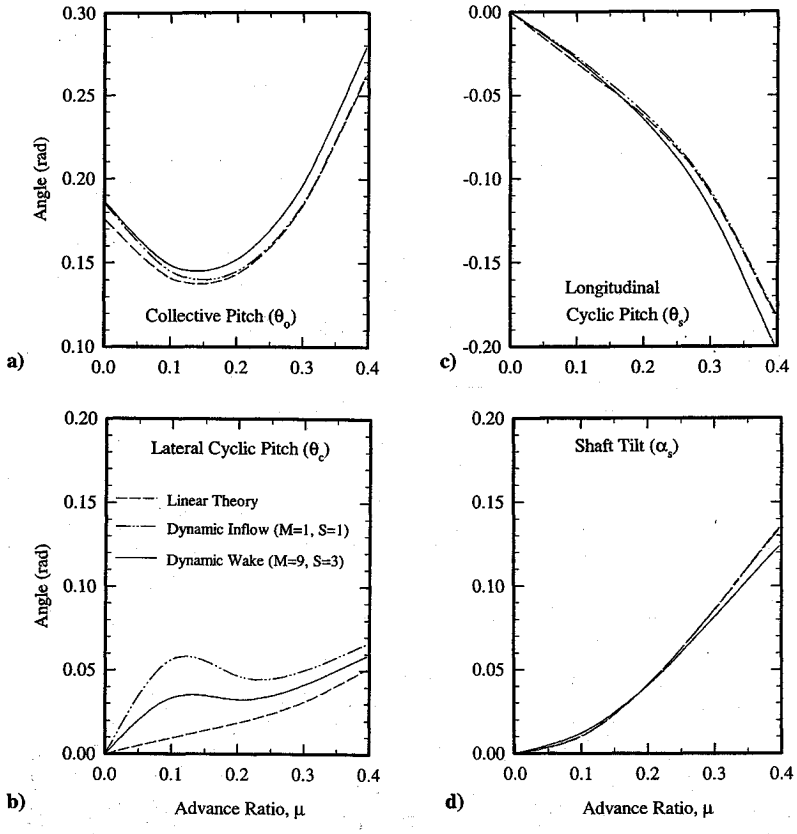

Fig. 8 Control inputs vs advance ratio from linear, dynamic inflow, and dynamic wake theories for $C_T/\sigma = 0.1$.

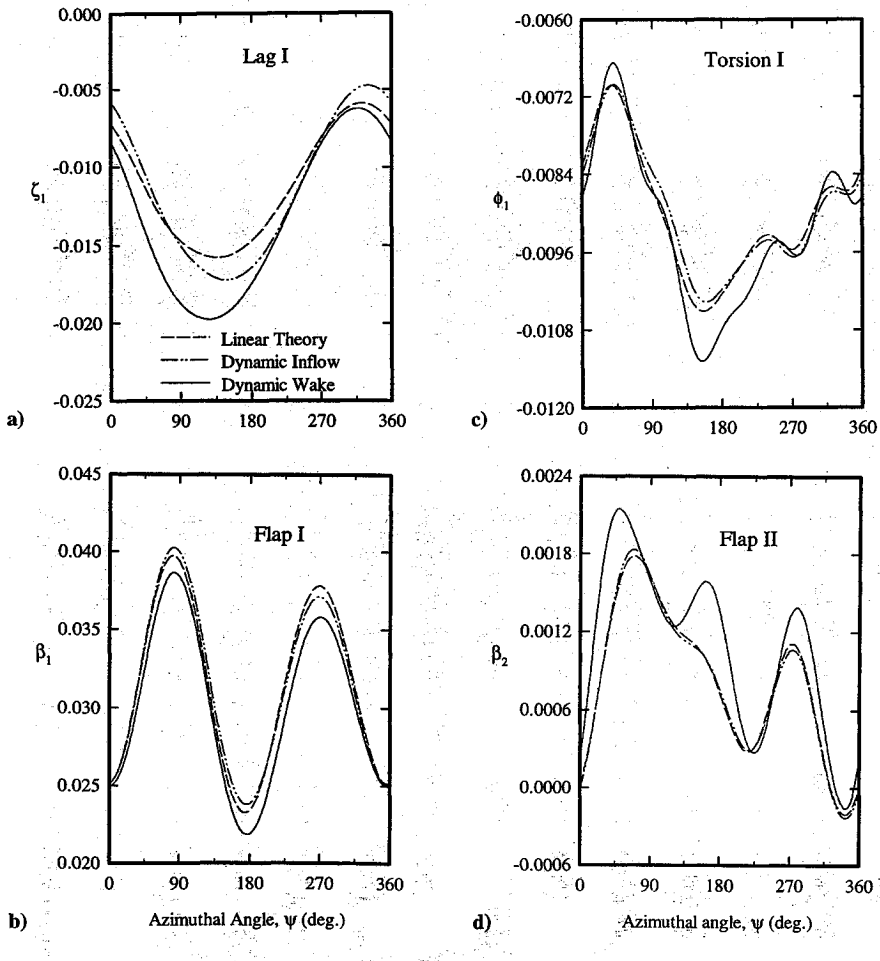

Fig. 9 Periodic response from linear, dynamic inflow ($M = 1, S = 1$), and dynamic wake ($M = 9, S = 3$) theories for $\mu = 0.4$ and $C_T/\sigma = 0.1$.

for each case two values of blade loading C_T/σ are considered, from a typical value of 0.1 to a very high value of 0.2. Overall, it is seen that for typical helicopter operations the dynamic inflow model agrees with the dynamic wake model with $M = 1$ and $S = 1$; hereafter we do not distinguish between these two models.

Figures 8 and 9, respectively, show the convergence characteristics of control inputs and periodic responses of trim analysis; they are based on three aerodynamic theories: linear, dynamic inflow, and dynamic wake theories. The control inputs θ_0, θ_c, θ_s, and α_s, and the periodic responses of the remaining four blade modes, except the second lag-bending and torsion modes, are shown. Convergence is obtained with $M = 9$ and $S = 3$; similar trim results for other combinations of M and S are not shown. In some cases convergence is not monotonic in that with a successive increase in the number of states in the wake representation, the convergence trend oscillates. For example, as seen from Fig. 8 at $\mu = 0.3$, the lateral cyclic pitch angle θ_c based on linear theory appreciably increases when dynamic inflow theory is used and then decreases with full-wake dynamics. Overall, Figs. 8 and 9 show the necessity of including full-wake dynamics in trim analysis; that is, a wake representation that goes well beyond dynamic inflow. We also mention the dominant influence of dynamic inflow and full-wake dynamics on θ_c at $\mu \approx 0.1$.

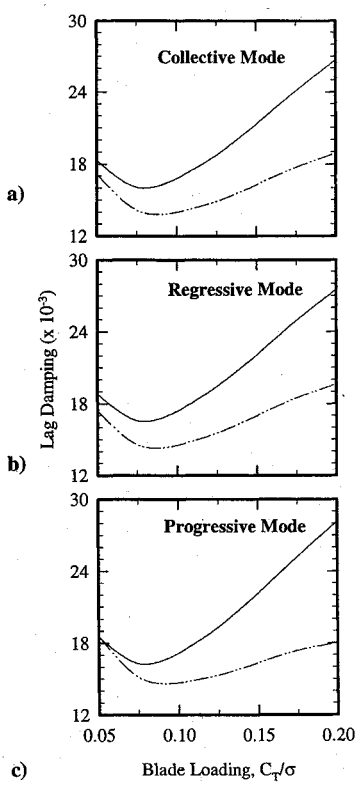

Fig. 10 Lag damping of the multiblade modes vs blade loading from dynamic inflow and dynamic wake theories for $\mu = 0.4$: —·—·—, dynamic inflow ($M = 1, S = 1$); ———, dynamic wake ($M = 9, S = 3$).

Parametric Studies

Figures 10–13 show the effects of four important parameters—thrust level, torsional flexibility, number of blades, and advance ratio—on the damping levels of different multiblade modes. Although lag damping is emphasized, damping levels of other modes from first flap bending to second torsion also are included (see Figs. 13a and 13b). This provides a relatively complete picture of the effects of full-wake dynamics on damping levels, in particular on first flap bending. Because dynamic inflow is widely used to approximate wake dynamics, the damping predictions with dynamic inflow also are included to facilitate direct comparison. Figure 10 shows lag damping of the multiblade modes vs thrust level C_T/σ; all three multiblade modes are included. Overall, it is seen that the inadequacy of the dynamic inflow representation increases with increasing thrust level. Similarly, Fig. 11 shows dynamic inflow vs full-wake dynamics for torsional frequency $\omega_\phi = 2.5$, 5, and ∞; that is, for increasing torsional stiffness. Here as well, the inadequacy of the dynamic inflow representation increases with increasing advance ratio at all torsional frequencies. Figure 12 shows lag damping for the collective, first-regressive, and first-progressive modes for four isolated rotors with $Q = 3$–6; differential-collective ($Q = 4$ and 6) and second-regressive and second-progressive ($Q = 5$ and 6) modes are not shown. For each rotor, the blade loading and solidity are kept constant at $C_T/\sigma = 0.2$ and $\sigma = 0.05$, respectively. With increasing number of blades and at any advance ratio, the damping levels decrease and become closer; this closeness is particularly evident for the collective and progressive modes. Perhaps this is due to the effects of closer wake spacing with increasing Q. But, for all four rotors, the qualitative aspect of damping variation with increasing μ remains the same.

Figure 13a shows the effect of dynamic wake on damping of all 18 multiblade modes of the 2-2-2 blade model. It is seen that the wake modeling should go well beyond dynamic inflow modeling with respect to all multiblade modes and at all advance ratios. The effects of blade modal representation on damping of multiblade modes of first and second flap-bending, lag-bending, and torsion degrees of freedom are investigated in Fig. 13b. The results

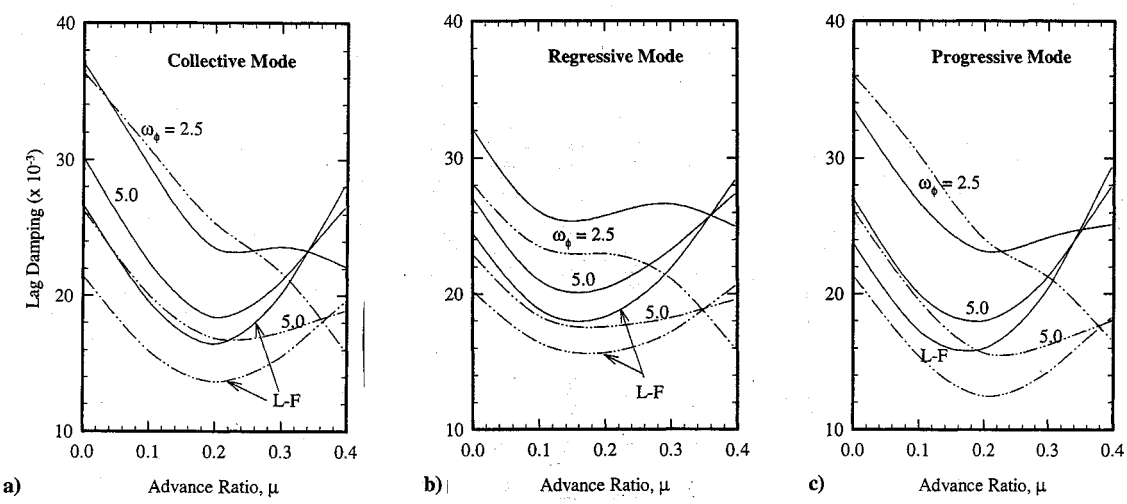

Fig. 11 Lag damping of the multiblade modes vs advance ratio for various torsional frequencies from dynamic inflow and dynamic wake theories for $C_T/\sigma = 0.2$: —·—·—, dynamic inflow ($M = 1, S = 1$); ———, dynamic wake ($M = 9, S = 3$).

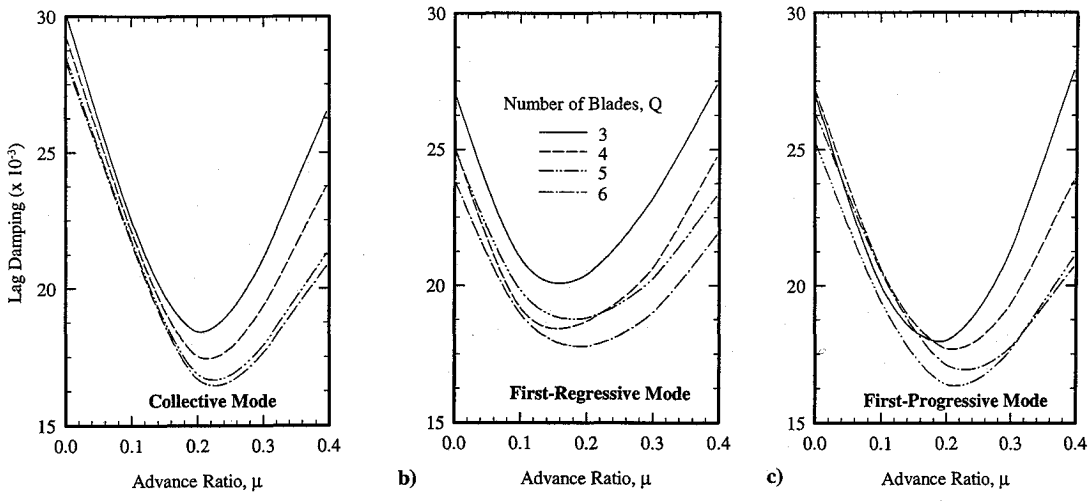

Fig. 12 Lag damping of multiblade modes vs advance ratio with increasing number of blades from dynamic wake theory ($M = 9, S = 3$) for $C_T/\sigma = 0.2$.

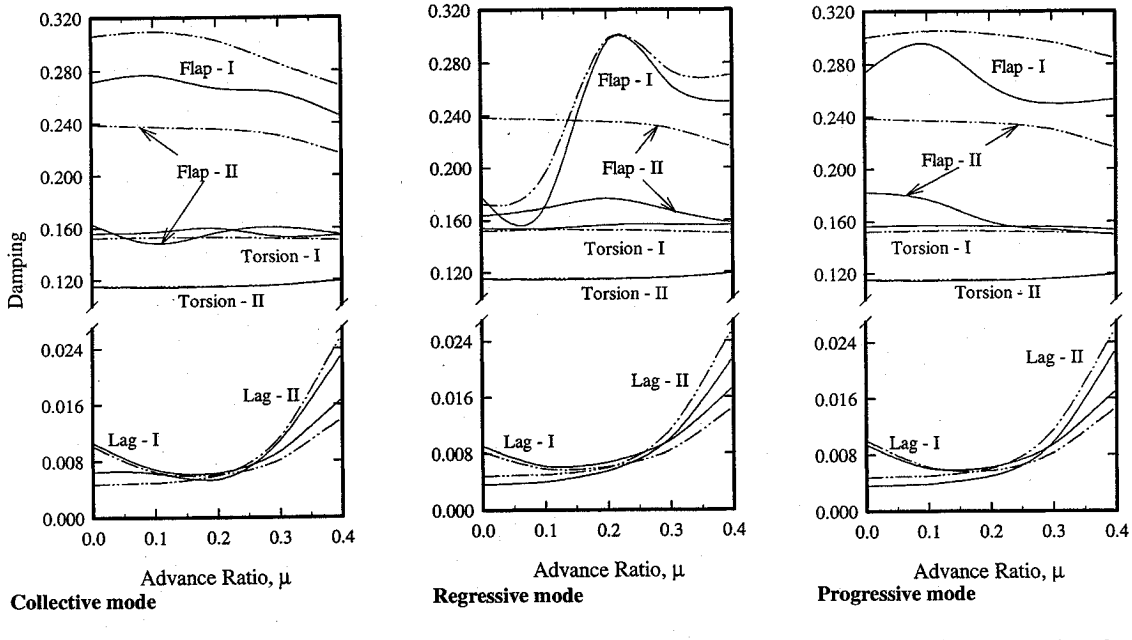

Fig. 13a Flap–lag–torsion damping of the multiblade modes vs advance ratio from dynamic inflow ($M = 1, S = 1$) and dynamic wake ($M = 9, S = 3$) theories for $C_T/\sigma = 0.1$: —·—·—, dynamic inflow; ———, dynamic wake.

are shown for 2-2-2, 3-3-3, and 4-4-4 blade models, and all three multiblade modes—regressive, collective, and progressive—are included. The results show that a 2-2-2 blade model gives virtually converged damping results from the low-frequency first lag to the high-frequency second torsion mode.

Correlation

The correlations with lag damping of the regressive mode are shown in Figs. 14 and 15. The predictions are based on four aerodynamic representations that vary from the linear theory to the dynamic wake theory with $M = 7, S = 3$, and $M = 9, S = 3$. The wake dynamics with $M = 9, S = 3$ (nine harmonics and three shape functions for each harmonic) gives converged results for all of the cases considered in this study. In fact, the wake representation with seven harmonics and three shape functions for each harmonic ($M = 7, S = 3$) also gives results that are almost identical to the converged results except at very high advance ratios ($\mu > 0.45$). It is included in Figs. 14 and 15 to demonstrate the convergence trends explicitly, and in the sequel we refer to only three aerodynamic theories: linear, dynamic inflow, and dynamic wake ($M = 9, S = 3$). The correlation in this investigation is confined to lightly and moderately loaded sections of the database[20]; blade loading C_T/σ based on linear theory ≤ 0.1, for which dynamic stall is not a major issue. The values of collective pitch angle θ_0 and shaft-tilt angle α_s are identified in respective figures.

Figure 14 shows the correlation with collective pitch $\theta_0 = 0$ deg and shaft angle $\alpha_s = 6$ and 8 deg from hovering to forward flight with advance ratio right up to 0.55. Consider $\alpha_s = 6$ deg (Fig. 14a). For $0 \leq \mu \leq 0.3$ the measured damping essentially remains constant; all three aerodynamic theories are virtually identical and agree with the data. This is because of low blade loading that varies from near-zero in hovering to about 0.02 at $\mu = 0.3$. For $0.3 \leq \mu \leq 0.55$, the thrust level varies from 0.02 to 0.06, and the data show that damping consistently increases with increasing advance ratio. It is during this latter phase of increasing damping that the differences among the three aerodynamic theories are observed. The linear theory is qualitatively inaccurate because it shows the trend of more or less constant damping. Inclusion of dynamic inflow appreciably improves the correlation. Dynamic wake brings further improvement over the dynamic inflow theory, and this improvement is equally appreciable. The correlation in Fig. 14b for shaft tilt $\alpha_s = 8$ deg is similar to that in Fig. 14a. In comparison with the linear theory, the improvements brought by dynamic wake are impressive and, overall, the correlation is good.

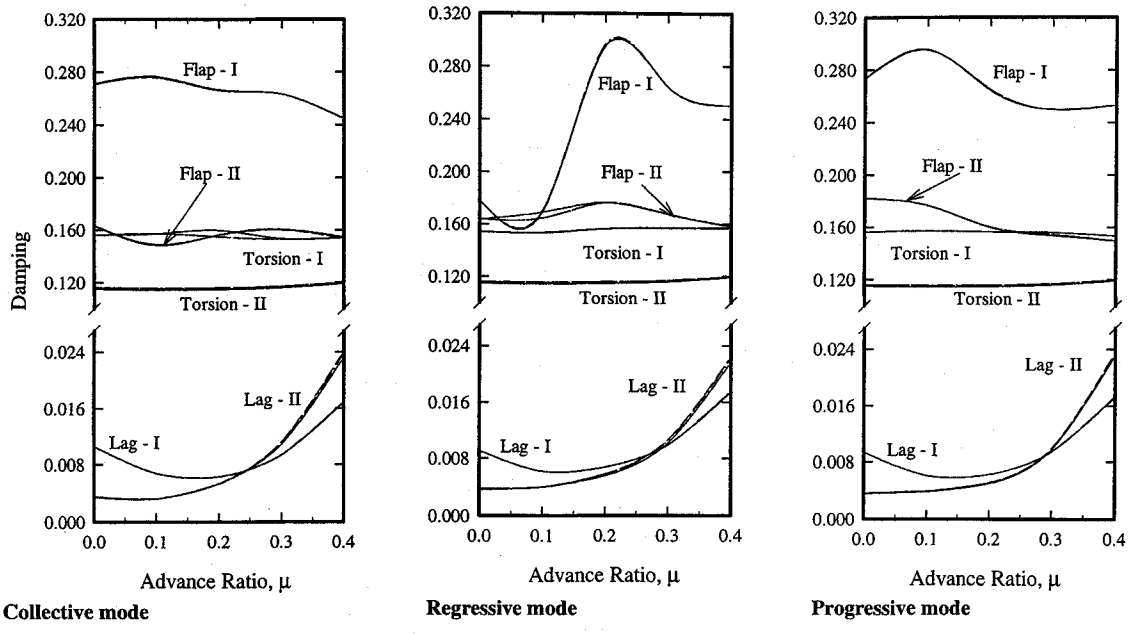

Fig. 13b Flap–lag–torsion damping of the multiblade modes vs advance ratio with dynamic wake ($M = 9, S = 3$) theory for various blade modal representations for $C_T/\sigma = 0.1$: ----, 4-4-4; -·-·-, 3-3-3; ———, 2-2-2.

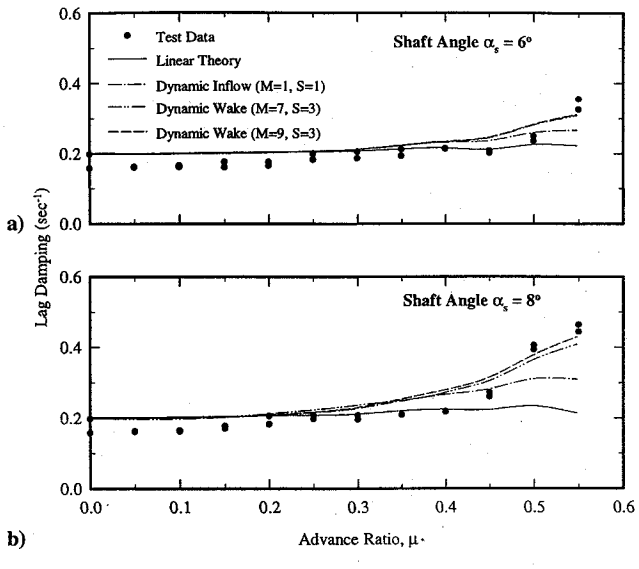

Fig. 14 Correlation of lag damping of the regressive mode with test data for collective pitch $\theta_0 = 0$ deg and shaft tilt $\alpha_s = 6$ and 8 deg.

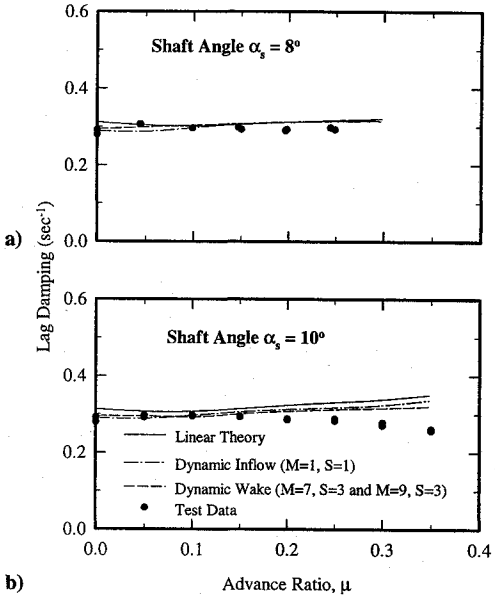

Fig. 15 Correlation of lag damping of the regressive mode with test data for collective pitch $\theta_0 = 3$ deg and shaft tilt $\alpha_s = 8$ and 10 deg.

The correlations with collective pitch $\theta_0 = 3$ deg are treated in Fig. 15a for $\alpha_s = 8$ deg and in Fig. 15b for $\alpha_s = 10$ deg. In Fig. 15a, the predictions from the three aerodynamic theories are virtually identical throughout; the data are available from hover to $\mu = 0.25$, and the correlation is good throughout. The thrust level C_T/σ remains low, from 0.03 in hovering to near-zero thrust condition at $\mu \approx 0.4$. Therefore, the role of downwash is relatively minor, and the agreement among the three aerodynamic representations and the excellent correlation from the linear theory are as expected.

Figure 15b shows the correlation for $\theta_0 = 3$ deg and $\alpha_s = 10$ deg. The data show that damping remains constant from hover up to an advance ratio $\mu = 0.2$, and the predictions from all three theories correlate well with test data; the dynamic wake and dynamic inflow theories give marginally better correlation. For $0.2 \leq \mu \leq 0.35$ the data show a slowly decreasing trend with increasing advance ratio. But all three theories predict that damping remains more or less constant. In the region $0.2 \leq \mu \leq 0.35$, where the data show a decreasing trend, the blade loading C_T/σ is nearly zero and dynamic stall is not a major issue.[22] Despite this, the inadequacy of the dynamic wake and inflow theories to predict this decreasing trend merits further investigation.

Conclusions

A complete three-dimensional, finite state wake representation is used in trim analysis to generate trim results of control inputs and periodic responses as well as in Floquet eigenanalysis to generate the damping levels. All of the multiblade modes from the low-frequency first-lag regressive mode to the high-frequency second-torsion progressive mode are included. The degree of wake and blade modeling that is necessary for converged results of trim and damping levels is studied. Such a modeling is used in parametric and correlation studies. These studies lead to the following conclusions.

1) For converged results, wake modeling requires at least three radial shape functions per harmonic and nine harmonics for fairly converged results. The number of harmonics and, to a lesser degree, the number of shape functions per harmonic needed for converged results increase with increasing blade loading, torsional flexibility,

and advance ratio. This means a wake representation that goes well beyond dynamic inflow is required.

2) Wake-dynamics effects on trim results and damping levels are appreciable from hovering to high advance ratios.

3) Overall, dynamic wake appreciably improves the correlation. For $\theta_0 = 3$ deg and $\alpha_s = 10$ deg, however, the data show that damping slowly decreases with increasing advance ratio. This slowly decreasing trend begins at a relatively low advance ratio ($\mu \approx 0.2$ or so) under near-zero thrust condition for which nonlinear effects, such as those due to dynamic stall, are not a major issue. This decreasing trend is not predicted by dynamic wake theory and merits further investigation.

Acknowledgments

The Army Research Office, Grant DAAL03-91-G-0007, and the U.S. Army Aeroflightdynamics Directorate (ATCOM), Grant NAG-2-797, sponsored the contributions of S. J. Chunduru, J. Nagabhushanam, and G. H. Gaonkar. P. Sampath of Hindustan Aeronautics Limited, India took keen interest during the progress of this investigation and offered several comments. We are grateful to him.

References

[1]Hohenemser, K. H., "Hingeless Rotorcraft Flight Dynamics," AGARD AG-197, Sept. 1974.

[2]Pitt, D. M., and Peters, D. A., "Theoretical Prediction of Dynamic-Inflow Derivatives," *Vertica*, Vol. 5, No. 1, 1981, pp. 21–34.

[3]Gaonkar, G. H., and Peters, D. A., "Review of Dynamic Inflow Modeling for Rotorcraft Flight Dynamics," *Vertica*, Vol. 12, No. 3, 1988, pp. 213–242.

[4]Peters, D. A., Boyd, D. D., and He, C. J., "Finite-State Induced-Flow Model for Rotors in Hover and Forward Flight," *Journal of the American Helicopter Society*, Vol. 34, No. 4, 1989, pp. 5–17.

[5]Peters, D. A., and He, C. J., "Correlation of Measured Induced Velocities With a Finite-State Wake Model," *Journal of the American Helicopter Society*, Vol. 36, No. 3, 1991, pp. 59–70.

[6]Peters, D. A., Barwey, D., and Su, A., "An Integrated Airloads-Inflow Model for Use in Rotor Aeroelasticity and Control Analysis," *Mathematical and Computer Modelling*, Vol. 19, No. 3/4, 1994, pp. 109–123.

[7]Manjunath, A. R., Nagabhushanam, J., Gaonkar, G. H., Peters, D. A., and Su, A., "Flap-Lag Damping in Hover and Forward Flight with a Three-Dimensional Wake," *48th Annual Forum Proceedings* (Washington, DC), The American Helicopter Society, Alexandria, VA, 1992, pp. 1061–1077; also *Journal of the American Helicopter Society*, Vol. 38, No. 4, 1993, pp. 37–49.

[8]Ravichandran, S., Gaonkar, G. H., Nagabhushanam, J., and Reddy, T. S. R., "A Study of Symbolic and Computational Aspects in Helicopter Dynamics," *Journal of Sound and Vibration*, Vol. 137, No. 3, 1990, pp. 495–507.

[9]Achar, N. S., and Gaonkar, G. H., "Helicopter Trim Analysis by Shooting and Finite Element Methods with Optimally Damped Newton Iterations," *AIAA Journal*, Vol. 31, No. 2, 1993, pp. 225–234.

[10]Nagabhushanam, J., and Gaonkar, G. H., "Automatic Identification of Modal Damping from Floquet Analysis," *Journal of the American Helicopter Society*, Vol. 40, No. 2, 1994, pp. 39–42.

[11]Johnson, W., "Recent Developments in the Dynamics of Advanced Rotor Systems—I," *Vertica*, Vol. 10, No. 1, 1986, pp. 73–107.

[12]Peters, D. A., and Su, A., "The Effect of Hidden Dynamic States of Floquet Eigenvalues," *Journal of the American Helicopter Society*, Vol. 35, No. 4, 1990, pp. 72–75.

[13]Friedmann, P. P., "Arbitrary Motion Unsteady Aerodynamics and Its Application to Rotary-Wing Aeroelasticity," *Journal of Fluids and Structures*, Vol. 1, No. 1, 1987, pp. 71–93.

[14]Torok, M. S., and Chopra, I., "Hingeless Rotor Aeroelastic Stability Analysis with Refined Aerodynamic Modeling," *Journal of the American Helicopter Society*, Vol. 36, No. 4, 1991, pp. 48–56.

[15]Kwon, O. J., Hodges, D. H., and Sankar, L. N., "Stability of Hingeless Rotors in Hover Using Three-Dimensional Unsteady Aerodynamics," *Journal of the American Helicopter Society*, Vol. 38, No. 2, 1991, pp. 21–31.

[16]Sharpe, D. L., "An Experimental Investigation of the Flap–Lag–Torsion Aeroelastic Stability of a Small Scale Hingeless Helicopter Rotor in Hover," NASA TP 2546, Aviation Systems Command (AVSCOM) TR 85-A-9, 1986.

[17]de Andrade, D., and Peters, D. A., "Correlation of Experimental Flap–Lag–Torsion Damping—A Case Study," *Mathematics and Computer Modelling*, Vol. 19, No. 3/4, 1994, pp. 135–158.

[18]Yoo, K. M., Hodges, D. H., and Peters, D. A., "An Interactive Numerical Procedure for Rotor Aeroelastic Stability Analysis Using Elastic Lifting Surface," *Proceedings of the Congress of the International Council of the Aeronautical Sciences* (Beijing, PRC), ICAS, Amsterdam, The Netherlands, 1992, pp. 1272–1280.

[19]Yoo, K. M., "Air-Resonance Analysis of Hingeless Rotor in Hovering Flight Using a 3-D Interblade Unsteady Wake Model," American Helicopter Society Aeromechanics Specialists Conf., Paper No. 7-2, San Francisco, CA, Jan. 1994.

[20]Gaonkar, G. H., McNulty, M. J., and Nagabhushanam, J., "An Experimental and Analytical Investigation of Isolated Rotor Flap-Lag Stability in Forward Flight," *Journal of the American Helicopter Society*, Vol. 35, No. 2, 1990, pp. 25–34.

[21]Cho, M. H., and Lee, I., "Aeroelastic Stability of Hingeless Rotor Blade in Hover Using Large Deflection Theory," *AIAA Journal*, Vol. 32, No. 7, 1994, pp. 1472–1477.

[22]Barwey, D., and Gaonkar, G. H., "Dynamic-Stall and Structural-Modeling Effects on Helicopter Blade Stability with Experimental Correlation," *AIAA Journal*, Vol. 32, No. 4, 1994, pp. 811–819.

[23]Manjunath, A. R., Nagabhushanam, J., Gaonkar, G. H., Chunduru, S. J., and Sampath, P., "Flap–Lag–Torsion Stability in Hover and Forward Flight with a Three-Dimensional Wake," American Helicopter Society Aeromechanics Specialists Conf., Paper No. 7-1, San Francisco, CA, Jan. 1994.

[24]Peters, D. A., "Toward a Unified Lift Model for Use in Rotor Stability Analyses," *Journal of the American Helicopter Society*, Vol. 30, No. 3, 1985, pp. 32–42.

[25]Barwey, D., "Dynamic Stall Effects on Hingeless Rotor Stability with Experimental Correlation," Ph.D. Dissertation, Dept. of Mechanical Engineering, Florida Atlantic Univ., Boca Raton, FL, April 1992.

[26]Peters, D. A., and Su, A., "Effect of an Unsteady Three-Dimensional Wake on Elastic Blade-Flapping Eigenvalues in Hover," *Journal of the American Helicopter Society*, Vol. 38, No. 1, 1993, pp. 45–54.